Flow around cactus-shaped cylinders

By Sharon Talley and Godfrey Mungal †

1. Motivation and objectives

This study combines biology and fluid mechanics to understand mechanisms that organisms use to cope with flows in their environment. Because organisms are selected in and by the flow conditions of their environment, their study can provide insight into novel mechanisms of controlling flow given certain constraints such as body size, basic shape (bluff vs. streamlined), and structural properties. Large desert succulents, such as the saguaro cactus, *Carnegiea gigantea* (Cactaceae), experience high wind velocities in their natural habitat and have converged on a common surface geometry of longitudinal cavities and spines (figure 1a). At the highest wind velocities in their natural habitat and when in danger of being uprooted by wind forces, saguaros with typical diameters of 0.5 m experience flows at Reynolds number (Re) up to 10^6. Being stationary organisms that must cope with high wind speeds from all directions, their shape is constrained to a cylindrical bluff body, and they likely rely on their complex surface geometry to affect the surrounding flow. Given that the shape and surface characteristics of an object influences the surrounding airflow, natural selection by wind may favor bluff body morphologies that reduce forces exerted by wind gusts (i.e. drag and fluctuating side-force). In this paper, we address the complex surface geometry of saguaros by experimentally examining the effect of longitudinal cavity depth on flow past circular cylinders ($Re \approx 2\times10^4$ to 2×10^5). Because of the broad nature of this interdisciplinary research, we provide background information on the physical attributes of saguaros, evidence of wind as a natural selective agent and flow around circular cylinders.

1.1. *Saguaro background*

The size, shape, surface characteristics and material properties prescribe a structure's (e.g. saguaro) ability to withstand high flow velocities. From a fluid mechanical perspective, saguaros can be viewed as giant cylindrical structures having complex surface geometry and a hemispherical free end. The main cylindrical trunks of adult saguaros reach heights of 8 m to over 15 m (Hodge 1991) and diameters of 0.3 m to over 0.8 m (Benson 1981). Age, climatic conditions and soil properties govern the size of saguaros; therefore, saguaro size can differ with environment. Information from one study area suggest that aspect ratios ($height/diameter$; h/d) of saguaros are height/ age dependent (Niklas and Buchman 1994). Saguaros taller than 4.5 m in height have (h/d) ratios between 12 and 23 and are relatively more slender than shorter saguaros, which have aspect ratios between 5 and 12 (h/d).

The complex surface geometry of saguaros is caused by longitudinal cavities and spines. Ten to 30 v-shaped longitudinal cavities (ribs) span the length of the trunk (Hodge 1991). The number of cavities depends on the trunk diameter; new cavities are added or deleted (figure 1a) to maintain a fraction cavity depth (l/d - depth of the cavity divided by the diameter of the cylinder) of 0.07 ± 0.0015 at approximately 1.5 m in height (Geller and

† Mech. Engg. Dept, Stanford University.

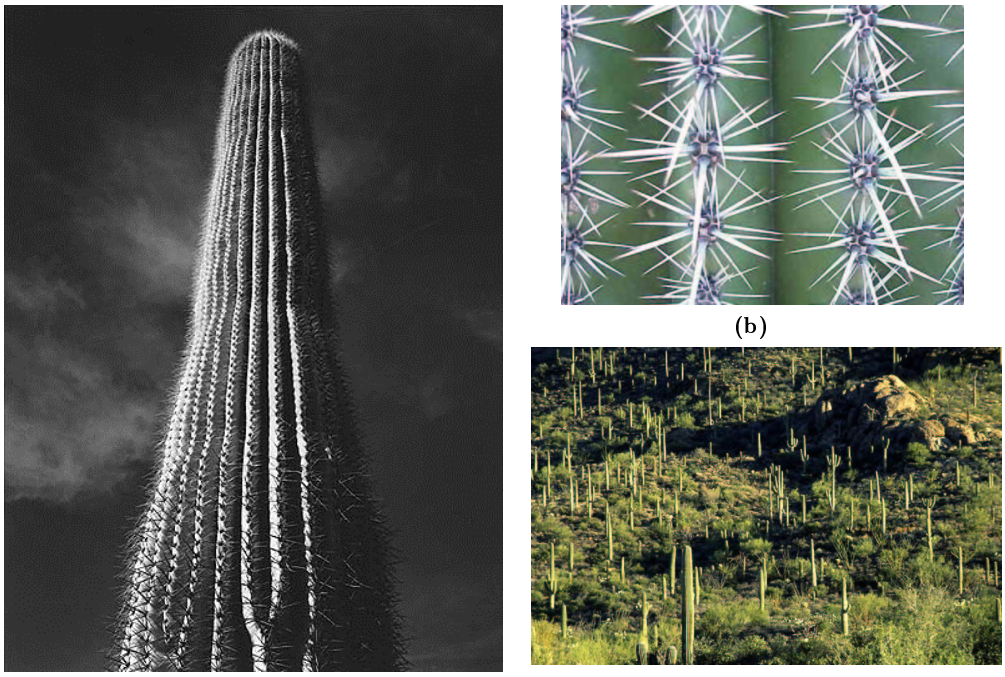

(a) (b) (c)

FIGURE 1. (a) Adult saguaro trunk showing the addition of cavities, (b) spines, and (c) saguaro forest

Nobel 1984). Cavity depth may increase higher up the trunk (personal observations). Cavity junctures (apices) have staggered clusters of 15 to 30 spines 2.5 to 7.6 cm long (Benson 1981; figure 1b).

Structural properties determine its load capacities and other factors that can interact with flow phenomena (natural resonance frequency and ability to flex causing aeroelastic responses). The root to soil interface likely determines a saguaro's load capacity, because toppled saguaros usually are found uprooted rather than broken at the trunk (see Talley *et al.* 2001 for structural strength of saguaro tissue). Saguaros have a shallow root system, which provides poor root anchorage and is believed to allow the toppling of saguaros during strong winds (Hodge 1991). While saguaros greater than a 1 m in diameter, may have natural frequencies between 4 and 10 Hz (Niklas 2002, personal communication), no studies have reported the forces required to topple saguaros, their behavior and flexibility in wind or their resonance frequency in soil. A morphologically similar species to the saguaro is the Mexican cardón, (*Pachycereus pringlei*), which has a more extensive root system of a deep bayonet-like central root and shallow lateral roots (Niklas *et al.* 2002). Anchorage is believed to be primarily provided by the central root system, which does not grow proportionately in girth or depth with growth of the trunk. Niklas (2002) argues that in an environment where water is extremely limited, as the cardón increases in size the root's function may shift more towards water absorption than anchorage because death by dehydration is more likely than toppling by wind. However, the likelihood of being toppled by wind depends on wind occurrences in their habitat, and other mechanisms may be responsible for their ability to withstand high wind velocities.

For wind to be a natural selective agent on saguaros, saguaros must be exposed to

wind, high wind velocities must occur in their habitat, and wind forces must affect their reproductive success. High wind velocities occur within the distribution of saguaros and frequently enough to affect their reproductive success. During a 9-year period, the maximum wind velocity recorded was 38 ms^{-1}, and velocities exceeding 22 ms^{-1} occurred almost every month (Bulk 1984; For a 0.5 m diameter saguaro, these wind velocities give Re of 1.3×10^6 and 7.3×10^5, respectively). The saguaro cactus can live for 150 years and requires 30 to 50 years to attain reproductive maturity, suggesting that high wind velocities need only occur every 30 to 50 years to be an important selective agent. Saguaros are likely exposed to winds because their desert habitat supports few if any other tall plants to provide shelter from the wind (figure 1c).

Substantial circumstantial evidence suggests that wind affects the reproductive success of saguaros by toppling them and causing their premature mortality (figure 1c, Benson 1981, Alcock 1985, Pierson and Turner 1998). It is likely that most of the saguaros that are toppled are large plants; however, enough young saguaros are toppled by wind to be documented (see figure 1c in Talley *et al.* 2001). Information on the occurrence of toppling events and on the wind velocities required to topple saguaros is lacking. The best-documented cases of mortality due to windfall are briefly mentioned in two different papers. (*i*) From 1941 to 1944, 2% of the saguaros in a 130 ha area were toppled by wind, and in 1945, 7% of the remaining saguaros in the same 130 ha area were toppled (Steenbergh and Lowe 1983). (*ii*) In August 1982, over 140 saguaros in a 15 ha area were toppled by wind velocities reported to be greater than 28 ms^{-1} (Pierson and Turner 1998). The fact that some saguaros are toppled by gusts, while many others remain standing is consistent with the natural selection scenario.

1.2. *Flow around circular cylinders*

Much is known about flows past circular cylinders, and below we provide a short review of flow phenomena relevant to the fluid mechanics of the saguaro's shape. Saguaros have the shape of a circular cylinder augmented with longitudinal cavities (the effect of spines is a future topic) and a hemispherical free end. For simplicity, we will focus flow around two-dimensional cylinders and then discuss free end effects. For an introduction to basic fluid mechanics, see White (1994, chapter 7).

Drag coefficient, C_D, curves of spheres and cylinders have four distinct Re flow ranges (figure 2a), which are distinguished by changes in C_D caused by boundary layer phenomena including separation and transition from laminar to turbulent flow (Roshko 1961, Achenbach 1977, Farell 1981). In the subcritical regime, the boundary layer is laminar and separates at an angle from the front stagnation point of about 80^o. In the critical regime, C_D drops as the laminar boundary layer separates further downstream (to about 100^o). The lowest C_D on the curve, occurring within the critical range, is the critical Re (figure 2a). At the critical Re, turbulent reattachment occurs, causing a bubble which delays separation (to about 140^o). In the supercritical regime, C_D rises as the reattachment bubble shrinks and moves upstream. In the transcritical regime, C_D is almost independent of Re and the boundary layer becomes turbulent before separation.

Comparisons of C_D curves of smooth and uniformly rough cylinders reveals that rough cylinders have C_D curves to the left of smooth cylinders and, therefore, experience the critical range at lower Re (Achenbach 1971). Roughness promotes turbulent transition (surface roughness size is quantified by the parameter k_s/d, the height of the roughness divided by the diameter of the cylinder), and generally, the greater the roughness, the greater the shift of the C_D curve to the left. Although a greater degree of uniform surface roughness promotes an earlier critical Re, it is accompanied by a smaller drop in C_D and

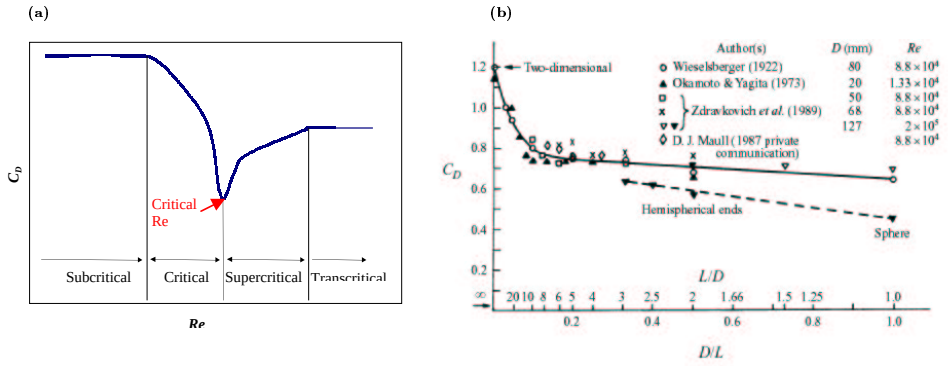

FIGURE 2. (a) Four ranges of flow past circular cylinders and (b) Drag coefficient of circular cylinders differing in aspect ratio of in terms of (Zdravkovich *et al.* 1989).

a shorter critical Re range. In addition, uniformly rough cylinders often have higher C_D than smooth cylinders in the postcritical ranges. Therefore, the C_D reduction afforded by uniform surface roughness occurs for a very limited Re range and at a cost of higher C_D in the postcritical regime.

Distributed surface roughness and complex surface geometries (i.e. dimples) can affect the shape of the C_D curve without the same limit in the range of C_D reduction and cost of higher C_D in the postcritical regime as occurs with uniformly rough cylinders. For example, distributed strips of roughness on cylinders promotes early transition without a rapid rise in C_D in the supercritical range (Nakamura and Tomonari 1982). Complex surface geometry, such as dimples on a cylinder (similar to those on a golf ball; Bearman & Harvey 1993), also induce early transition and extend the critical range. The dimpling geometry may be effective at tripping the laminar boundary layer while inhibiting the thickening of the turbulent boundary layer (Mehta and Pallis 2001). Thus, C_D depends not only on the size of surface roughness but also on the shape (geometry) and distribution of surface roughness. Although many surface modifications have been studied to reduce drag on circular cylinders, to our knowledge, none have examined spanwise v-shaped cavities with l/d greater than 0.035. Our study is motivated by the saguaro cactus and other tall succulents that have a l/d of 0.07. In this paper, we compare unsteady drag and lift of smooth and uniformly rough cylinders ($k_s/d = 1.74 \times 10^{-3}$ and 8.41×10^{-3}) to cylinders differing in cavity depth ($l/d = 0.035$, 0.07, 0.105).

Cylinders with free ends generally have lower C_D than two-dimensional cylinders (figure 2b; Zdravkovich *et al.* 1989). The effect of free ends on C_D depends on aspect ratio. For $l/d < 1$, the lower the aspect ratio the greater the effect of the free ends. For cylinders with both ends free, free-end effects appear to be beneficial for aspect ratios (h/d) < 30. This may also be the case for cylinders with one free end; Fox, Apelt, and West (1993) reported that at an aspect ratio equal to 30 there is still a considerable decrease in the mean and fluctuating forces. The average aspect ratio of saguaros is unknown; however, aspect ratios likely range between 5 and 23 (h/d). Therefore, the effect of free ends should not be discounted. The saguaro has one free end that is hemispherical. Note that in figure 2b, hemispherical ends give a larger decrease in C_D than flat ends. Cavities on the hemispherical free end, such as those on a saguaro, may provide even a larger decrease in C_D than a smooth-hemispherical free ends.

1.3. *Significance*

With our interdisciplinary approach, we address the fluid mechanics of a novel surface geometry and fundamentals in biology. This is the first study to our knowledge to examine how spanwise v-shaped cavities (l/d up to 0.105) can affect flow around cylinders. Research on the effect of surface augmentation on flow around bluff bodies is important to many applications, such as chimneystacks, towers, and marine risers. In biology, fundamental concepts in evolutionary ecology are addressed by examining whether natural selection by wind has optimally shaped stationary organisms to reduce potentially damaging wind forces (drag and fluctuating side-force). Surprisingly few have studied the fluid mechanics of biological organisms, especially terrestrial and stationary organisms, with bluff bodies. No studies have reported accounts that bluff-bodied organisms reduce drag by surface roughness (Vogel 1981). Surface roughness has been argued an unlikely adaptation to control drag, because the reduction in C_D afforded by the surface roughness is accompanied by an increase in C_D at higher Re (Denny 1988 and Vogel 1981). However, an increase in C_D in a Re range that is rarely, if ever, experienced by the organism in question should have no effect on its evolution. Moreover, complex surface roughness affects the C_D curve differently than uniform roughness, and other forces and flow phenomena (i.e. drastic changes in C_D, fluctuating side-forces, and vibration frequencies) may be important but overlooked selective agents on the shape of organisms.

2. Experimental arrangement and methods

2.1. *Test cylinders*

Circular cylinders 76.2 cm in length (cylinders spanning the tunnel) and 57.5 cm in length (flat-capped, free-ended cylinders) were manufactured from RenShape 460 modeling board. All cylinders were 9.98 cm in diameter. Six surfaces were examined: one smooth, two uniformly rough ($k_s/d = 1.74 \times 10^{-3}$, 8.41×10^{-3}), and three different depths of 24 spanwise v-shaped cavities ($l/d = 0.035$, 0.07, and 0.105). Uniform roughness, $k_s/d = 1.74 \times 10^{-3}$ and 8.41×10^{-3}, was provided by commercial 100 and 36 grit sandpaper, respectively. Sheets of sandpaper were attached to the smooth cylinder with double-sided adhesive tape, adding a thickness less than 2 mm. The sandpaper spanned the cylinder to $\pm 130^o$ with respect to the flow direction (0^o). The 24 cavities on the cylinder were 15^o apart cut at included angles of 124^o, 82.5^o, and 60^o for the 0.035, 0.07, and 0.105, respectively.

2.2. *Experimental arrangement in wind tunnel*

Figure 3 shows the experimental configuration. Experimental measurements were performed in a low-speed blower tunnel with a test section 76.2 cm high by 76.2 cm wide at flow velocities from 4 to 29.5 ms^{-1} ($Re \approx 2 \times 10^4$ to 2×10^5). Geometric blockage was 13% ($d/$ width of the test section). In all experiments, cylinders were mounted vertically between aluminum endplates (3.35 mm thick). To eliminate direct contact between endplates and cylinders, endplates were fixed 2.54 cm below the roof and 2.54 cm above the floor. Endplates were $8d$ long by $7d$ wide with a distance between the cylinder axis and the leading edge of $3.5d$ (Szepessy 1994). Aspect ratio between the endplates was 7.08 (h/d) for cylinders spanning the tunnel and 5.47 (h/d) for cylinders with free ends. The portion of all cylinders that were between the endplate and the closest wall (i.e. 0.066 for cylinders spanning the tunnel and 0.033 for free-ended cylinders) had a smooth surface, and their contribution was neglected in the force calculations.

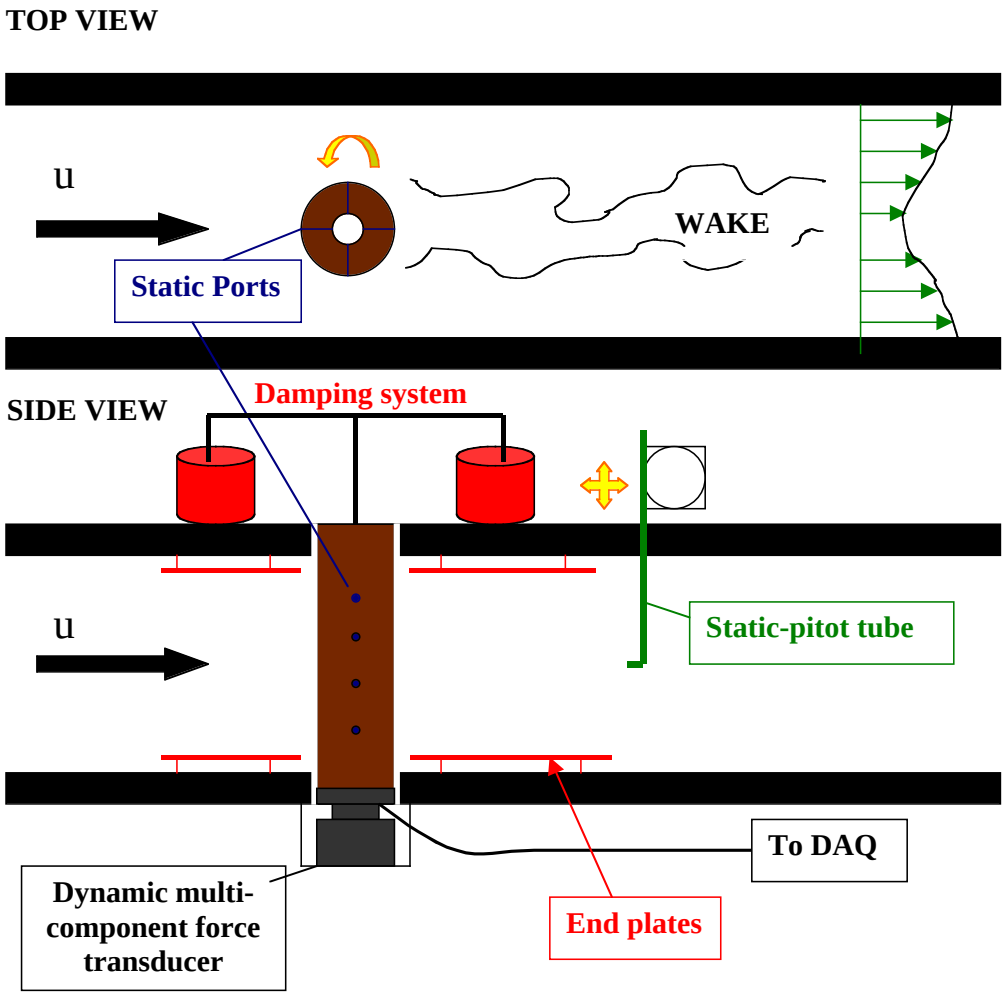

FIGURE 3. Experimental configuration.

2.3. *Pressure distribution*

Cylinders were equipped with at least 16 static-pressure ports of less than 1-mm diameter. At 19.1 cm, 31.8 cm, 44.5 cm, and 57.2 cm from base of the cylinders, there were a series of four static ports located 90^o apart from one another. For cylinders with cavities, the 16 static ports were located on the middle of the cavity wall. Cavity cylinders were equipped with two additional static ports 44.5 cm from the base, one of which was located on the apex of the cavity juncture and the other in the trough (valley) of the cavity. The three static-port locations along the cavities were used to determine pressure differences with the different orientations of the cavity to the flow. Only the cylinders spanning the tunnel were measured for pressure distribution. Cylinders were mounted on a turntable and rotated 15^o between sampling periods. Pressure measurements were made using a differential pressure transducer at a sampling rate of 500 Hz for a total of 150,000 samples for each velocity.

2.4. *Direct force and vortex shedding measurements*

Force measurements were obtained directly using a dynamic multi-component force transducer (MC3A-6-250, Advanced Mechanical Technology, Inc, Watertown, MA). The cylinders were attached to a metal plate that was directly attached to the force transducer. The transducer was rigidly attached to the tunnel. The MC3A-6-250 transducer has six channels; three channels measure forces in the three directions (drag, lift, and weight) and three channels measure moments about the different directions. Channels have a 2% or less crosstalk which had to be corrected for due to the cylinder length creating large moments, and hence, causing considerable errors in force measurements. Correction factors were obtained through comprehensive calibrations using a pulley system and a series of weights. Wires were attached to the cylinder at three or more different spanwise locations (to correct for moment crosstalk contribution) for both the drag and lift directions.

The MC3A-6-250 transducer is not rigid and allowed the cylinder to displace (approximately 1 cm) when under maximum wind loads. To prevent large amplitude vibrations due to vortex shedding, the free end of the cylinders spanning the tunnel (ends were outside the tunnel roof; figure 3), was attached to a floating dampening system. No corrections were made for damping in the force calculations. No damping system was employed for free-ended cylinders (see discussion). Using a spectrum analyzer, we measured the resonance frequencies of the cylinders. Cylinders spanning the tunnel had a natural frequency of 8 Hz, and the flat-capped cylinders had a natural frequency of 20 Hz.

The mounting mechanism did not allow different orientations of the cavities to the flow, so all cylinders had the cavity apices facing the flow. A total of 150,000 samples at a sampling rate of 500 Hz were measured for up to 30 different velocities (from 4 to 29.5 ms^{-1}) for each cylinder. Velocity was obtained using a Pitot-static tube attached to a differential pressure transducer. Vortex-shedding frequency (f) was measured by counting the peaks of the fluctuating lift forces and presented as the Strouhal number ($St = f^{*}d/U$, where U is the velocity). Blockage corrections were made for the C_D and velocity calculations using formulas from Allen and Vincenti (1944). Blockage corrections were not applied to the lift coefficient, C_L. The root-mean-square (r.m.s.) lift coefficient, $C_{L'}$ was calculated using the r.m.s. of the lift fluctuations (L').

3. Results

3.1. *Pressure distribution*

Pressure distributions at $Re = 110{,}000$ for the cylinders spanning the tunnel are shown in figure 4a. There is greater pressure recovery for cylinders with cavities than for the smooth and rough cylinders. The cylinders with cavities have greater negative pressures on the sides of the cylinder. Pressure recovery appears to increase with increasing cavity depth while the negative pressures on the sides of the cylinder appear not to be affected by cavity depth. The pressure distribution depends somewhat on the orientation of the cavity to the flow. When the cavity trough faced the flow, static pressures were very similar to those when the wall faced the flow. Conversely, when apex was facing the flow, static pressures differed from those when the wall or cavity trough faced the flow. The largest differences were for pressures on the front and sides of the cylinders. figure 4b shows the pressure distribution at different locations along the cavity for the 0.07 l/d cylinder.

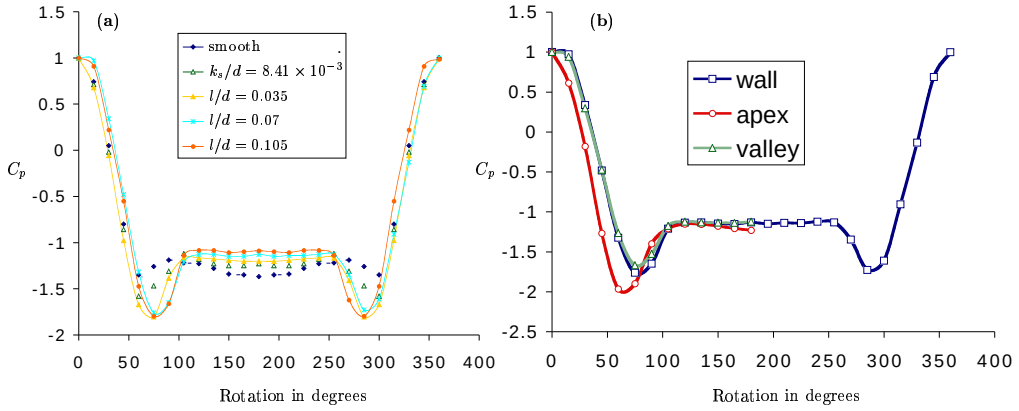

FIGURE 4. (a) pressure distribution of all cylinders at *Re* 110,000 and (b) pressure distribution from different locations along the cavity for the 0.07 l/d cylinder.

3.2. *Drag, lift and vortex shedding*

C_D vs. *Re* for the test cylinders are shown in figure 5. Note that C_D values were calculated using only the portion of the cylinder between the endplates (neglecting the smooth portions of the cylinder between the endplate and the nearest wall) and, therefore, the C_D values are higher than those reported elsewhere. However, trends in the magnitude of the drop in C_D and the critical *Re* for the two uniformly rough cylinders are in close agreement with those reported in Güven, Farell, and Patel (1980). The cavity cylinders have no obvious critical *Re*. At the highest *Re*, the C_D for the cavity cylinders asymptotically approaches C_D values of 1.13, 1.09, 1.04 for the 0.035, 0.07, and 0.105 l/d cylinders, respectively.

$C_{L'}$ plotted against *Re* is shown in figure 6a. The $C_{L'}$ values for a smooth cylinder are in agreement with those reported in Norberg (2001). The cavity cylinders had lower values of $C_{L'}$ than the smooth and the $k_s/d = 8.41 \times 10^{-3}$ cylinder. The cavity cylinders had lower values of $C_{L'}$ than the $k_s/d = 1.74 \times 10^{-3}$ cylinder from *Re* of 2.0×10^4 to 1.0×10^5. The $k_s/d = 1.74 \times 10^{-3}$ cylinder had the lowest $C_{L'}$ values from *Re* of 1.2×10^5 to 1.6×10^5. For the two uniformly rough cylinders, the lowest $C_{L'}$ value corresponds to their critical *Re*. Plots of unsteady drag and lift as a function of time (1 s) for different *Re*, show that variation is a function of vortex-shedding frequency and the natural frequency of the model. For all the cavity cylinders and the $k_s/d = 1.74 \times 10^{-3}$ cylinder, the variation in drag and lift was dominated by the vortex-shedding frequency. Conversely, for the smooth and $k_s/d = 8.41 \times 10^{-3}$ cylinder, the variation in drag had a greater amplitude of lower frequencies that mirrored the natural resonance frequency of the model (data not shown). *St* plotted against *Re* for the test cylinders is shown in figure 6b. There is little variation in *St* with *Re* for all cylinders. The cylinders with cavities have slightly higher *St* from *Re* 2×10^4 to 6×10^4. No trends with C_D and $C_{L'}$ curves were obvious.

3.3. *Free-end effects*

Drag coefficients of flat-capped cylinders were less than their corresponding two dimensional cylinders (figure 7a); however, the trends in C_D curves for flat cylinders were similar to the trends of their corresponding two-dimensional cylinders. The flat-capped cylinders had no damping system. Consequently, cylinders experienced oscillations aris-

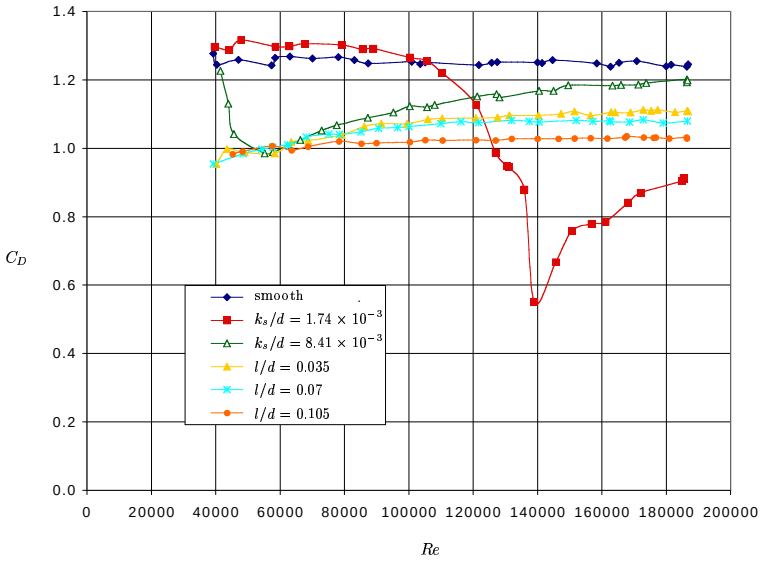

FIGURE 5. C_D vs Re for two-dimensional cylinders.

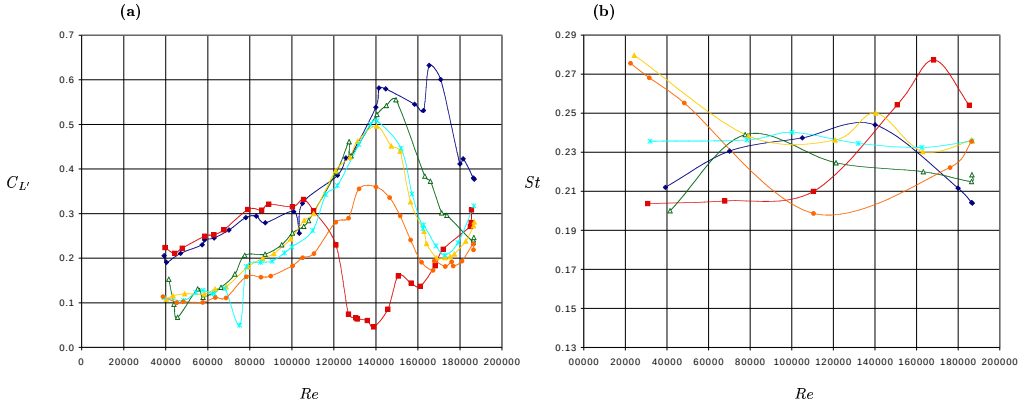

FIGURE 6. (a) $C_{L'}$ vs Re for two-dimensional cylinders and (b) St vs Re for two-dimensional cylinders (legend see figure 5).

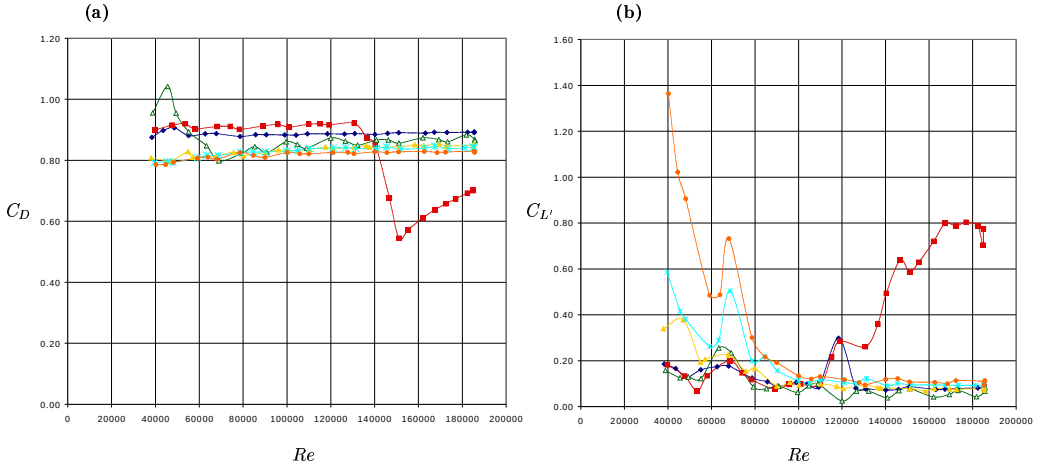

FIGURE 7. (a) C_D vs Re for free-ended cylinders and (b) $C_{L'}$ vs Re for free-ended cylinders (legend see figure 5).

ing from the lack of stiffness in the force transducer. The large amplitude vibrations of the resonance frequency likely affected the $C_{L'}$ curves (figure 7b) and vortex shedding.

4. Discussion

4.1. *Pressure distribution*

The greater pressure recoveries for cylinders with cavities than for smooth and rough cylinders suggests a decrease in drag for cylinders with cavities. The pressure recoveries differed slightly with location of the static port along the cavity and orientation of the cavity to the flow. When the apex of cavity juncture faced the flow, there were greater negative pressures on sides of the cylinders and slightly less pressure recovery, indicating slightly higher drag.

4.2. *Drag, lift and vortex shedding*

In general, an increase in cavity depth causes a decrease C_D. Over the entire Re range (2×10^4 to 2×10^5), the cylinders with cavities had lower C_D values than the smooth cylinder. Conversely, before their critical range, both uniformly rough cylinders had higher C_D values than the smooth cylinder. The cylinders with cavities had lower C_D values than the rough $k_s/d = 8.41\times 10^{-3}$ cylinder with the exception of small Re range from 5×10^4 to 7×10^4 where all had equal values. For Re up to 1.2×10^5, the cavity cylinders had lower C_D values than the $k_s/d = 1.74\times 10^{-3}$ cylinder. Although roughness, $k_s/d = 1.74\times 10^{-3}$, caused a larger C_D reduction at higher Re, cavities induce a lower C_D at lower Re and the reduction is sustained as C_D is almost independent of Re. Analogous to surface roughness, the cavities likely serve to trip turbulent transition but at an lower Re. The flat curves of the cavity cylinders have no obvious critical Re, which suggests that the transition to turbulence occurred at Re less than 2×10^4. The fact that C_D does not drop rapidly with Re (as it does for the uniformly rough and smooth cylinders) may be biologically important to saguaros because rapid changes in force can damage a structure. The extent of the C_D reduction at higher Re remains unanswered. We suspect that the cavities have flow benefits up to Re on the order of 10^6, because this range of C_D reduction likely corresponds to potentially damaging Re that saguaros commonly experience in their natural habitat with a possible added safety factor for those rarer, higher velocity gusts (30 ms^{-1}). For example, if a 0.5 m diameter saguaro commonly experiences gusts of 22 ms^{-1} and is likely to experience a top gust of 30 ms^{-1} at least once every 30 years, the C_D of saguaros is likely to have C_D reductions extending to 7×10^5 and possible further.

C_D values of saguaros may be influenced by factors not examined in this study. Depending on the orientation of the cavities to the flow, the C_D values for cavity cylinders likely differ somewhat from those reported in figure 5. When the cavity or cavity walls are facing the flow compared to the apex facing the flow, there is less negative pressures at the sides of the cylinders and base pressure recovery is slightly better. Since we tested only with cavity apices pointing into the flow for all cavity cylinders, the C_D values may be somewhat overestimated. We also expect that axial flow and angle of attack may be important factors in the drag reducing capability of cavities on saguaros. It is conceivable that the cavities induce axial flow (which may be induced from the free end). For cylinders spanning the tunnel, axial flow was most likely inhibited because cavities were filled in at the ends of the cylinders making the cylinders smooth between the endplates and the closest wall. Visualization experiments carried out in a low-speed smoke tunnel

suggest that longitudinal cavities affect axial flow and the symmetry of vortex shedding (Talley *et al.* 2001).

For the entire *Re* range, the cavity cylinders had a lower magnitude of fluctuating side-force than the smooth cylinder, and this was almost always the case for the $k_s/d = 8.41 \times 10^{-3}$ cylinder. For *Re* up to 1.1×10^5, the cylinders with cavities had a lower magnitude of fluctuating side-force than the $k_s/d = 1.74 \times 10^{-3}$ cylinder. The ability to dampen fluctuating side-forces may be particularly important in keeping saguaros upright since large fluctuations in forces may break or dislodge roots. Variances in the unsteady drag and fluctuating side-forces correspond to the vortex shedding. All cylinders were attached to the same damping system and corrections were not made for damping and differences in the weights of the cylinders. The natural frequency of all cylinders was ≈ 8 Hz and resonance contributed slightly to variations in the unsteady drag and fluctuating side-forces. For the cavity cylinders and the $k_s/d = 1.74 \times 10^{-3}$ cylinder, the natural frequencies were less evident in the waveforms of the unsteady drag and fluctuating side-forces. The differences in amplitudes at resonance frequencies excited by vortex shedding needs to be investigated further.

4.3. *Free-ended cylinders*

The reduction in drag due to free-end effects is likely due to the low aspect ratio of the flat-capped cylinders (5.5 h/d). In nature, aspect ratios of saguaros likely fall between 5 and 23 (h/d). Free-end effects on drag have been shown to be important for aspect ratios (h/d) < 30 (Zdravkovich *et al.* 1989), suggesting that end effects may be important for saguaros. Furthermore, hemispherical ends, such as those on saguaros, are likely to have even a greater effect on drag reduction (figure 2b). Longitudinal cavities may promote axial flow (Talley *et al.* 2001) and hemispherical caps with longitudinal cavities may cause even a further reduction in drag and fluctuating side-forces. This will be addressed in future studies.

Results for the flat-capped cylinders were obtained without a damping system. Recall that the force transducer used for the measurements lacks stiffness, allowing the cylinder to vibrate. In order to reduce structural vibration interactions with vortex shedding, a damping system needs to be employed. For the free-end cylinders, it is difficult to attach a damping system without affecting the flow conditions at the free end. Several attempts were made to control vibrations without affecting flow around the free end, but none were successful. We lowered the natural frequency of the model by filling the model with lead and copper; this brought the natural frequency down from 20 to 10 Hz; however, the amplitude was still great enough to interfere with the measurements. Next, we tried elastic dampers by making rubber, neoprene, and cork gaskets that varied in thickness; however, the benefit afforded by the elastic damping was counteracted by hysteresis effects. We also attached a damping system to the sides of the cylinder using piano wires that were pulled tight with weights (figure 8a). This added stiffness to the lift direction, but did not greatly improve the amplitude of the resonance vibrations. We stiffened the same system by using thicker wire in the tunnel and rods outside the tunnel, but this allowed only marginal improvement in the lift direction and no improvement in the drag direction.

5. Future studies

A new damping system will be employed to control natural resonance (figure 8b). Because the damping system will affect flow around the free end, experiments will be

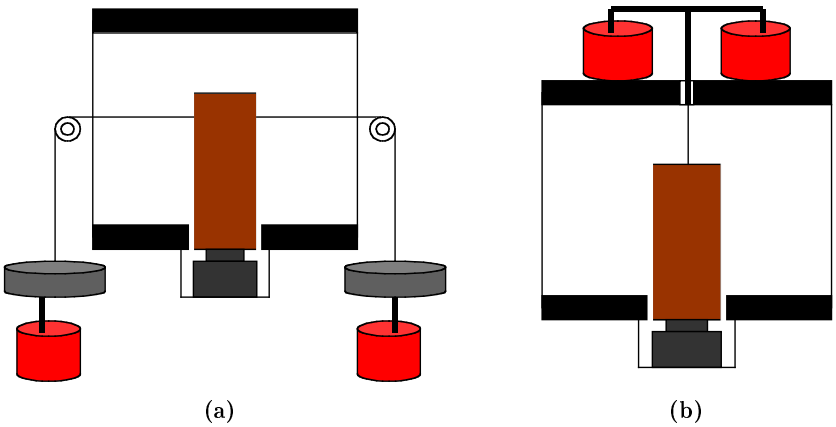

FIGURE 8. Damping systems (a) with wires and weights and (b) with rod from ceiling of tunnel.

performed with and without a damping system. Further work is required to assess the effect of longitudinal cavities in the range of Re relevant to the saguaro as well as with models that allow axial flow (i.e. hemispherical caps). Future experiments will obtain C_D curves over a range of Re from 2×10^4 (for computational comparisons) to 1×10^6 (limit of wind velocities in the saguaro habitat) and will include the effect of hemispherical caps and spines. Research may also include angle of attack, flexibility of the body and vortex induced vibrations.

Much about the physical characteristics of saguaros and their behavior in the wind remains elusive. Simple field measurements of aspect ratio and longitudinal changes in cavity depth need to be made. For structural interactions with wind, the natural frequency of a saguaro cactus needs to be measured in their natural habitat (sandy and/or rocky soils) both under dry and wet conditions. Saguaros may have mechanisms to avoid vortex shedding frequencies coming into resonance with the natural bending frequencies. Simple video recordings of the saguaro during the monsoon, will provide information on the behavior of the saguaro in high wind velocities. Structural deformations and motion of the saguaro in wind may add or alleviate forces caused by the wind. Furthermore, bending of the saguaro stem in the wind may increase axial flow in cavities and my alleviate pressure recovery at the base.

6. Acknowledgements

This work is sponsored by the Center for Turbulence Research, Stanford University and NASA Ames. We are grateful to everyone that has made this work possible. We especially thank Dr. Parviz Moin, Dr. Peter Bradshaw, Dr. Nagi Mansour, Dr. John Eaton, Dr. Rabindra Mehta, Ross Bishop, Dr. Georgi Kalitzin, Ralf Socher, Gianluca Iaccarino, Larry Siebold, Alex Hsu, Loren Rideout, Simon Song, Bruce MacGregor, Vijay Somandepalli, Dr. Haecheon Choi, Dr. Javier Jiménez, Dr. Joel H. Ferziger, Tamer Zaki, and Gorazd Medic.

REFERENCES

Achenbach, E. 1971 Influence of surface roughness on the cross-flow around a circular cylinder. *J. Fluid Mech.* **46**, 321-335.

Achenbach, E. 1977 The effects of surface roughness on the heat transfer from a circular cylinder to the cross flow of air. *Int. J. Heat Mass Transf.* **20**, 359-362.

Alcock, J. 1985 *Sonaran Desert Spring.* University of Chicago Press.

Allen, H. J. & Vincenti, W. G. 1944 Wall interference in a two-dimensional-flow wind tunnel, with consideration of the effect of compressibility. *NACA Report* 782.

Bearman, P. W. & Harvey, J. K. 1993 Control of circular cylinder flow by the use of dimples. *AIAA J.* **31**, 1753-1756.

Benson, L. 1981 *The Cacti of Arizona.* The University of Arizona Press.

Bulk, H. C. 1984 The Maximum Daily Wind Gust Speed Climatology at Sky Harbor Airport, Phoenix Arizona. *The Laboratory of Climatology, Arizona State Univ. Report* 18.

Denny, M. W. 1988 *Biology and the Mechanics of the Wave-Swept Environment.* Princeton University Press.

Farell, C. 1981 Flow around fixed circular cylinders: fluctuating loads. *ASCE J. Eng. Mech. Div.* **107**, 565-573.

Fox, T. A., Apelt, C. J. & West, G. S. 1993 The aerodynamic disturbance caused by the free-ends of a circular cylinder immersed in a uniform flow. *J. Wind Eng. Ind. Aerodyn.* **49**, 389-400.

Geller, G. N. & Nobel, P. S. 1984 Cactus ribs: influence on PAR interception and CO_2 uptake. *Photosynthetica* **18**, 482-494.

Gibson, A. C. & Nobel, P. S. 1986 *The Cactus Primer.* Harvard University Press.

Güven, O., Farell, C. & Patel, V. C. 1978 Surface-roughness effects on mean flow. *J. Fluid Mech.* **98**, 673-701.

Hodge, C. 1991 *All About Saguaros.* Hugh Harelson/Arizona Highways, Phoenix.

Mehta, R. D. & Pallis, J. M. 2001 Sports ball aerodynamics: effects of velocity, spin and surface roughness. *Materials and Science in Sports Conference*, Coronado, CA.

Nakamura, Y. & Tomonari, Y. 1982 Effects of surface roughness on the flow past circular cylinders at high Reynolds numbers. *J. of Fluid Mech.* **123**, 363-378.

Niklas, K. J. 2002 Wind, size, and tree safety. *J. Arboric.* **28**, 84-93.

Niklas, K. J. & Buchman, S. L. 1994 The allometry of saguaro height. *Am. J. Bot.* **81**, 1161-1168.

Niklas, K. J., Molina-Freaner, F. Tinoco-Ojanguren, C. & Paolillo, D. J. 2002 The biomechanics of *Pachycereus pringlei* root systems. *Am. J. Bot.* **89**, 12-21.

Nobel, P. S. 1994 *Remarkable Agaves and Cacti.* Oxford University Press.

Norberg, C. 2001 Flow around a circular cylinder: Aspects of fluctuating lift. *J. Fluids Struct.* **15**, 459-469.

Pierson, E. A. & Turner, R. M. 1998 An 85-year study of saguaro (*Carnegiea gigantea*) demography. *Ecology.* **79**, 2676-2693.

Roshko, A. 1961 Experiments on the flow past a circular cylinder at very high Reynolds number. *J. Fluid Mech.* **10**, 345-356.

Steenbergh, W. F. & Lowe, C. H. 1983 *Ecology of the Saguaro III.* National Park Service.

Szepessy, S. 1994 On the spanwise correlation of vortex shedding from a circular cylinder at high Reynolds number. *Phys. Fluids* **6**, 2406-2416.

Talley, S., Iaccarino, G., Mungal, G. & Mansour, N. 2001 An experimental and computational investigation of flow past cacti. *Annual Research Briefs*. Center for Turbulence Research, NASA Ames/Stanford Univ., 51-63.

Vogel, S. 1981 *Life in Moving Fluids.* Princeton University Press.

Zdravkovich, M. M., Brand, V. P., Matthew, G. & Weston, A. 1989 Flow past short circular cylinders with two free ends. *J. Fluid Mech.* **203**, 557-575.